10th International Conference on Fracture Mechanics of Concrete and Concrete Structures
FraMCoS-X
G. Pijaudier-Cabot, P. Grassl and C. La Borderie (Eds)
https://doi.org/10.21012/FC10.233583

INVESTIGATIONS OF SIZE EFFECT IN CONCRETE DURING SPLITTING USING DEM CPMBINED WITH X-RAY MICRO-CT SCANS

JAN SUCHORZEWSKI[*†] AND JACEK TEJCHMAN[†]

[*] The Swedish Cement and Concrete Institute (CBI), Research Institutes of Sweden
Brinellgatan 4, 501-15 Borås, Sweden
e-mail: jan.suchorzewski@ri.se, www.ri.se

[†] Gdańsk University of Technology
Narutowicza 11/1, 80-233 Gdańsk, Poland
e-mail: tejchmk@pg.edu.pl, www.pg.edu.pl

Key words: Concrete, size effect, fracture, microCT, DEM

Abstract: A size effect is a fundamental phenomenon in concrete materials. It denotes that both the nominal structural strength and material brittleness always decrease with increasing element size under tension. The objective of the paper is to investigate a mechanical size effect in plain concrete. The focus was on meso-structural phenomena contributing to different failure modes in the post-peak region. The experimental programme was carried out on concrete specimens of the diameter *D*=74, 100, 150, 200 and 250 mm during tensile splitting. The strength and ductility of specimens decreased with increasing specimen diameter. The concrete meso-structure was determined with the very advanced x-ray micro-tomography system and was next implemented into numerical calculations. The size effect calculations were performed for all experimental concrete specimens with the three-dimensional spherical discrete element model YADE. Concrete was depicted as a four-phase composite material including aggregate, cement matrix, interfacial transition zones (ITZs) and macro-voids. 2D and 3D calculations were performed. The process of micro- and macro-cracking was studied in detail for three various failure modes, including the quasi-brittle, brittle and snap-back behaviour. The macroscopic stress-CMOD curves and shapes of cracks were directly compared with the laboratory test outcomes. The evolutions of broken contacts, normal and tangential displacements were elaborated at the aggregate level.

1 INTRODUCTION

The splitting tensile tests (also known as the Brazilian tests) are the most popular laboratory tests on concrete to determine its uniaxial tensile strength due to their loading and specimen shape simplicity [1]. This test consists of applying a distributed compressive force along the length of a concrete cylinder, which induces a primarily tensile stress perpendicular to the loading plane of the specimen's cross-section with sharp compressive stress near the points of load application. The splitting tensile strength is generally greater than the direct tensile strength and lower than the flexural strength.

A splitting tensile test on concrete is subjected to a size effect depending on the cylindrical specimen diameter (Fig.1) and the width of loading/supporting strips. The size effect is characterised by both the strength and ductility reduction with increasing concrete specimen diameter. It is greater for wider loading/supporting strips. The size effect on strength in this test is mainly due to heterogeneous fracture as a result of a non-uniform distribution of the horizontal tensile stress caused by compression stresses at loading/supporting regions [2-6].

The experimental campaign was performed to measure the size effect both on strength and brittleness, combined with micro-CT scans. The micro-CT is a 3D imaging technique using x-rays to create cross-sections of a physical object that is next used to recreate a virtual model (3D model) without destroying the original object [7-9]. The x-ray micro-tomography system Skyscan 1173 has been applied that represents a new generation in high-resolution desktop X-ray micro-tomography systems. As compared to usual X-ray micro-tomography systems, our scanner has two basic advantages: a) large specimens up to 200 mm in diameter may be scanned and b) the specimens are scanned with a higher precision (2-3 microns). Note that a continuous investigation of the entire fracture process under deformation with the X-ray micro-tomography system (without breaks for scanning) was not possible for technical reasons yet [3].

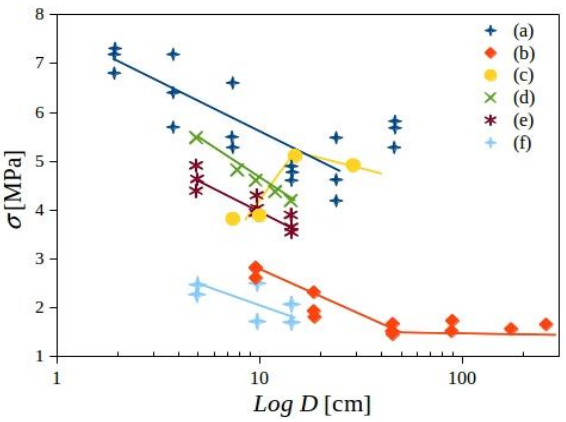

Figure 1: Relationship between maximum tensile stress $\sigma=2Pmax/(\pi DL)$ and specimen diameter D (in logarithmic scale) in splitting tensile tests on plain concrete from laboratory experiments: a) Bažant et al. [2], b) Hasegawa et al. [3], c) Carmona et al. [4], d) Kadlecek et al. [5] and e) and f) Torrent [6] (continuous lines are trend lines) (P - vertical splitting force, D - specimen diameter, L - cylindrical specimen length).

Three concrete specimens with various sizes were scanned by micro-CT. Based on the scans, the original meso-structure was implemented in the discrete element method (DEM). The stress-strain curves were directly compared with experimental outcomes. The crack patterns and broken contacts were analysed for different specimen diameters with various failure modes.

2 EXPERIMENTAL CAMPAIGN

2.1 Specimens and test procedure

The experiments on concrete during splitting tension were carried out with the diameter of cylindrical specimens D=74, 100, 150, 192 and 250 mm. Two plywood boards as loading strip were used and scaled proportionally with the specimen diameter. The strength and ductility decreased with increasing specimen diameter. For large specimens D>100 mm, a clear snap-back occurred. The strain maps were obtained with the digital image correlation (DIC) technique for various specimen diameters. A micro-cracking process was observed with the digital microscope. The interfacial transition zones (ITZs) were investigated by a scanning electron microscope. The specimens were sawed out from one concrete block with the dimension 200×200×20 cm3 after 28 days from casting to obtain results independent of drying and shrinkage [10]. The maximum aggregate diameter was 16 mm. The *w/c* ratio was equal to 0.77 and the sand point was 43.7%.

The specimens were loaded with loading/supporting strips according to European Standard [11]. The hardboard with the dimensions: b=15 mm and t=4 mm for D=150 mm was used. For other diameters, the strips width b was proportionally scaled with the diameter (b/D=const.) to avoid the influence of boundary conditions [13]. The static loading machine ZWICK Roaller Z400 was used that was equipped with a crack opening extensometer (Sandner EXR10-2x) with the maximum error of 2%. The extensometer was located at the mid-height of the concrete specimen and glued to the specimen front side. The quasi-static tests were performed under the CMOD-control

(CMOD - crack mouth opening displacement) with the displacement rate of 1×10-5 mm/s. The CMOD-time relationship was perfectly linear in all tests.

2.2 Results

The horizontal normal tensile stress versus the normalised crack opening is presented in Fig.2. The clear decrease of strength with increasing diameter was observed. The large specimens were apparaently more brittle. The specimen of the diameter *D*=74 mm had the average tensile strength of σ=4.35 MPa, of *D*=100 m - σ=3.55 MPa, the standard diameter of *D*=150 mm - σ=3.22 MP and the largest specimen with *D*=250 mm, σ=2.8 MPa.

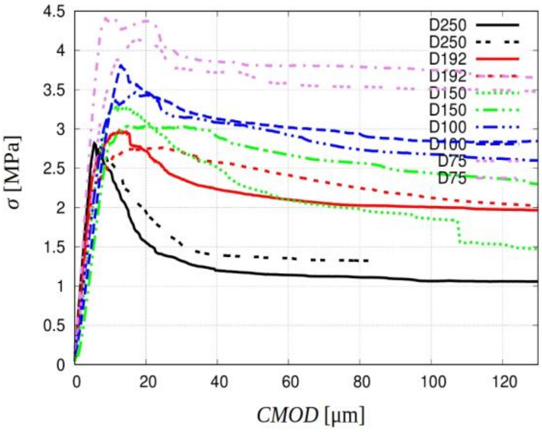

Figure 2: Evolution of horizontal tensile stress $\sigma=2P_{max}/(\pi DL)$ versus CMOD displacement in splitting tension with different specimen diameter *D*.

Figure 3 presents the evolution of the horizontal tensile stress σ versus the normalized vertical displacement *v/D* for the different specimen diameter. The results' scatter decreased with increasing specimen diameter *D*. Apart from the decreasing strength, the brittleness increased significantly after the peak load. For the specimens *D*=74 mm and *D*=100 mm, it was characterised by an increasing displacement after the peak while for *D*=150 mm, *D*=196 mm and *D*=250 mm by a decreasing displacement after the peak (snap-back behaviour).

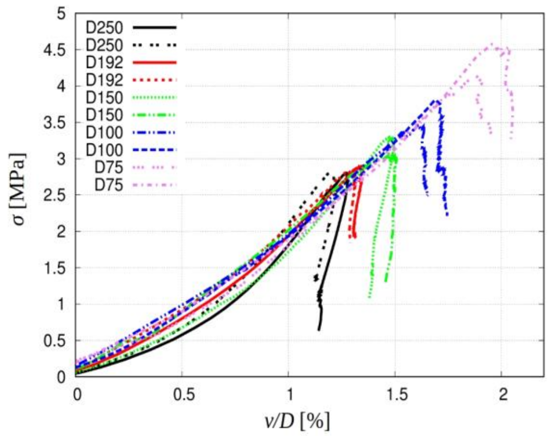

Figure 3: Evolution of horizontal tensile stress $\sigma=2P_{max}/(\pi DL)$ versus normalized vertical displacement *v/D* in splitting tensile tests for different specimen diameter *D*.

2.3 Micro-CT scans of fracture

All concrete specimens were scanned with the same setting parameters. The X-ray source voltage of the micro-CT scanner was set to 130 keV, the current was 61 µA and exposure time was equal to 2000 ms. The pixel size of the micro-CT was 39,68 µm. The X-ray projections were recorded with the rotation increment of 0,2^{o} within 180^{o}. To reduce the noise in the captures X-ray projections, the frame averaging option was set to be 4 and random movement option was 10. The scanning time was approximately 6 hours. One specimen of each diameter was scanned with micro-CT before loading. Then the specimen was loaded until CMOD=200 µm and scanned again. The mid-region of the specimen *D*=74 mm was carefully analysed and compared with the undamaged state.

The basic three phases of concrete were determined from 3D micro-CT images: aggregate, cement matrix and macro-voids. Moreover, the aggregate size distribution and pore structure were analysed. The segmentation was performed with the CTAn 1.17.7.2 software delivered by the firm SkyScan Bruker (the producer of the micro-tomograph). The bottom and top threshold used for each phase was: 0-63 (pores and cracks), 63-112 (cement matrix) and 112-255 (aggregate). After a thresholding procedure, fine particle “despeckle” was used to remove the objects finer than 10 voxels (in volume) except pores. The crack surfaces of all specimens were segmented and the cracks’ volume was determined. Some cracks were connected with inner pores during fracture that increased the cracks’ volume. For the specimen D=74 mm, the main crack was the most curved (Fig.4a). The crack did not propagate through aggregates. The total crack volume was V=117.10 mm^3 and the average crack width was w=0.19 mm. The crack in the specimens D=150 mm and D=250 mm was less curved and exhibited typical wedges at the top and bottom of the specimens under the loading/supporting strips (Fig.4b-4c). The crack volumes were V=103.53 mm^3 and V=78.74 mm^3 and the average crack widths w=0.086 mm and w=0.039 mm for the specimens D=150 mm and D=250 mm. Moreover, in the specimen D=250 mm, the crack had a few fine branches in the zones ahead of wedges (Fig.4c). The crack volume and average crack width decreased with increasing specimen diameter. In the specimens with D>74 mm, the crack intersected 6 (D=150 mm) and 11 aggregate particles (D=250 mm).

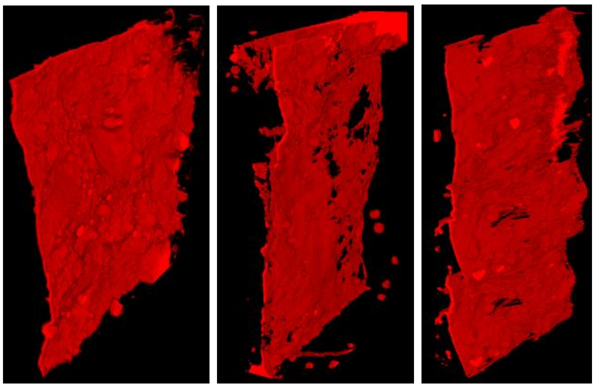

a) b) c)

Figure 4: 3D image of crack for specimens: a) D=74 mm, b) D=150 mm and c) D=250 mm after test.

During the experiments, the clear size effect occurred with respect to strength (Fig.5). The tensile strength decreased by 15% for the small specimens from σ=4.4 MPa (D=74 mm) down to σ=3.6 MPa (D=100 mm). The strength’s decrease was the smallest for the largest specimens (by 3% between D=192 mm and D=250 mm). The results of own experiments on splitting tension were compared with the size effect law by Bazant’s (SEL type I for unnotched specimens) [13]. The parameters of the size effect were calibrated for D=150 mm (f_t=3.13 MPa): B=5.40 and D_0=5.39 (Fig.5). The experimental results were in good agreement with a theoretical solution [13] except the largest specimen D=250 mm wherein the strength’s reduction was smaller by 30% than that predicted by SEL.

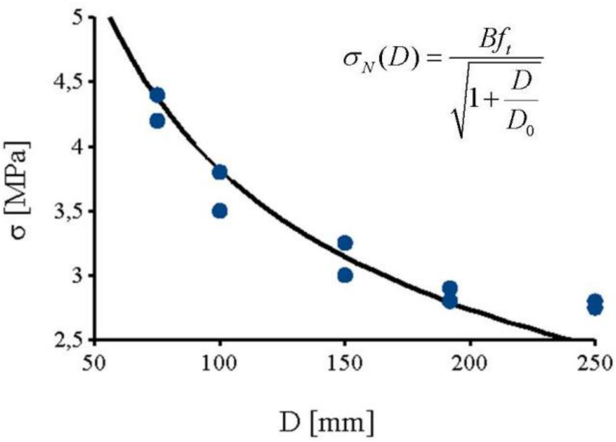

Figure 5: Comparison between experiments and SEL type I by Bažant [14]: tensile strength σ versus specimen diameter D.

3 DEM RESULTS

The laboratory experiments described in Section 2 were simulated with DEM. A stochastic distribution of aggregates was taken into account due to micro-CT images for three specimen diameters D=74 mm, D=150 mm and D=250 mm. The full 3D micro-CT scan was possible before the test solely for the smallest specimen D=74 mm due to size limitations in the micro-CT system (Fig.6).

The following parameters of the cohesion and tensile strength were used in all DEM analyses of tensile splitting independently of the specimen diameter D (calibrated on accompanying uniaxial compression tests): cement matrix ($E_{c,cm}$=15 GPa, C_{cm}=140 MPa and T_{cm}=25 MPa) and ITZs ($E_{c,ITZ}$=12 GPa, C_{ITZ}=112 MPa and T_{ITZ}=20 MPa). ITZs were obviously the weakest phases. The ratio $E_{c,ITZ}/E_{c,cm}$=0.8 was chosen based on the experiments by Xiao et al. [14]. The remaining ratios were also assumed as 0.8: C_{ITZ}/C_{cm}=0.8 and T_{ITZ}/T_{cm}=0.8 due to the lack of experimental results. Note that there were no contacts between aggregate grains with d_a>2 mm. The remaining parameters were constant for all phases and regions: υ_c=0.2 (Poisson's ratio of grain contact), μ=18^o (inter-particle friction angle) [15], α_d=0.08 (damping parameter) and ρ=2.6 g/cm3 (mass density). The prescribed damping parameter α_d and velocity did not affect the results during bending [9]. In the case of α_d<0.08, the too excessive kinetic energy was always created during fracture. The effect of the α_d-value on global results for $\alpha_d \geq 0.08$ became insignificant. The calculated mean nominal inertial number I for the maximum vertical load (that quantifies the significance of dynamic effects) was <10^{-4} that always corresponded to a quasi-static regime.

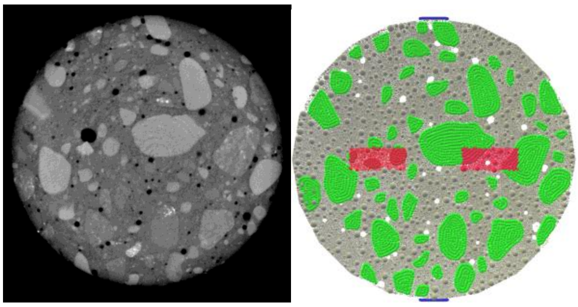

a) b)

Figure 6: Concrete specimen of D=74 mm a) micro-CT scan and b) DEM model.

The DEM results for splitting are shown in Figs.7-9. Very good agreement was achieved between numerical and experimental results for all specimens diameters with respect to the stress-displacement curve (Fig.7) and fracture geometry (Fig.9). The calculated maximum tensile splitting stress $\sigma=2P_{max}/(\pi DL)$ decreased (as in the experiments) with increasing diameter D. For D=74 mm, the calculated tensile splitting strength was f_t=4.0 MPa for v/D=1.8% (Fig.7Aa), for D=140 mm, f_t=3.2 MPa for v/D=1.5% and f_t=2.8 MPa for v/D=1.2% (D=250 mm, Fig.7Ca). Apart from the smallest specimen D=74 mm, where the DEM strength was smaller by 4% than the lower experimental result (Fig.7Ab), the remaining DEM results were between the experimental curves. For the specimen D=250 mm, the strength obtained with DEM (Fig.7Ca) was equal to the higher experimental result (Fig.7Cc).

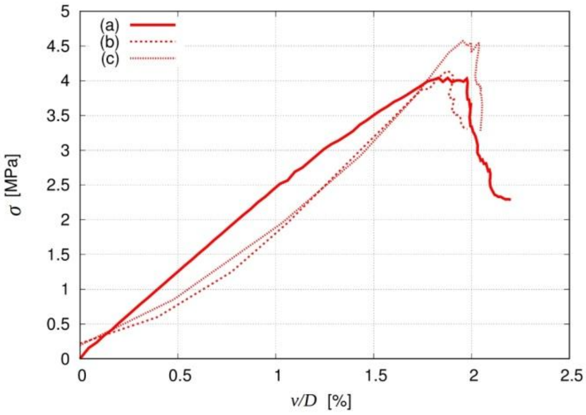

A)

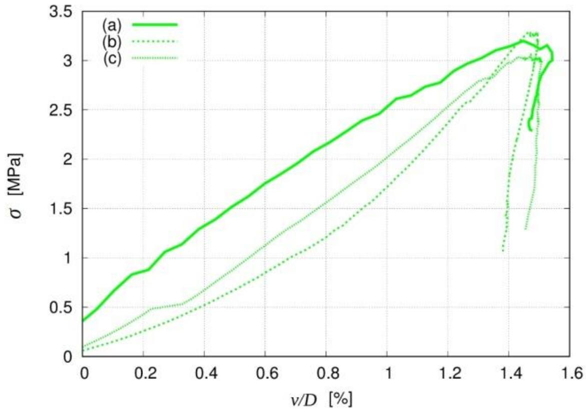

B)

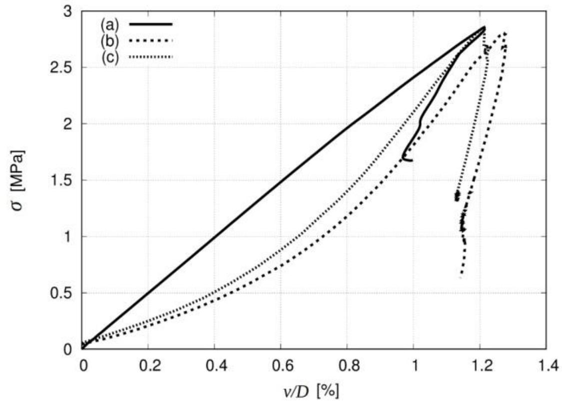

C)

Figure 7: Tensile stress σ versus normalized displacement v/D for splitting tension: a) DEM and b)- and c) experiments for different specimen diameters

(A) D=74 mm, B) D=150 mm and C) D=250 mm).

The elastic response of the DEM model was similar as in the experiment, however, the initial hardboard compression-hardening response was not well reproduced (since the loading boards were assumed in DEM as rigid). The concrete brittleness increased with increasing specimen diameter. A clear snap-back mode of failure occurred for specimens D>74 mm, expressed by a simultaneous reduction of the vertical stress σ and vertical piston displacement v after the maximum stress σ_{max}. The calculated rate of softening was similar as in the experiment for the specimens D=74 mm and D=150 mm. For the largest specimen D=250 mm, the calculated softening was higher than in the experiment.

The damage process in DEM was described by a number of broken contacts n (Fig.8). The broken contacts were divided on those broken in ITZs (Fig.8a), in the cement matrix (Fig.8b) and the total number of broken contacts (Fig.8c). The amount of contacts broken in ITZs up to the peak was equal to 57%, 62% and 68% for D=74 mm, D=150 mm and D=250 mm respectively (Fig.8a). For the specimen D=150 mm (Fig.8B) in an elastic part of the curve, fast creation of macro-crack is visible as an increase of broken contacts number (mainly in cement matrix). It is connected with an instant crack appearance between the two largest aggregate grains in the specimen centre. After the peak, the increase of broken contacts in the cement matrix was greater than in ITZs by the factor of 5. The normalized total number of broken contacts in peak increased with the specimen diameter and was equal to n/D=17.5 for D=74 mm (Fig.8A), n/D=22 for D=150 mm (Fig.8B), n/D=28 for D=250 mm (Fig.8C). Those specimens were more damaged before the peak and thus had the lower strength.

Finally, the cracks geometries in deformed specimens (Fig.9b) were compared with the micro-CT scans (Fig.9a). For the specimen D=250 mm, the image from the digital camera of full specimen height was additionally presented as the specimen was too high for full scanning (2/3 of the total specimen height was scanned with micro-CT).

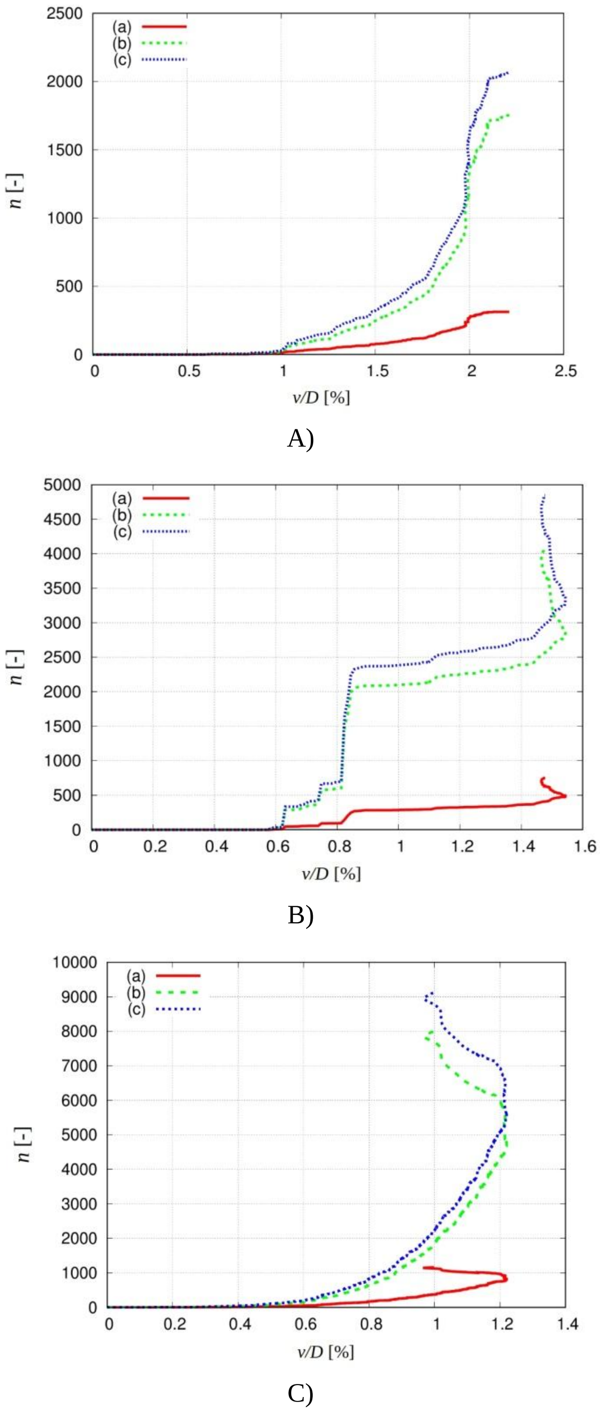

Figure 8: Number of broken contacts n against normalized displacement v/D for splitting in DEM: a) ITZ, b) cement matrix, c) all particles for different specimen diameter D (A) D=74 mm, B) D=150 mm and C) D=250 mm).

For the specimen D=74 mm (Fig.9A), the crack propagated close to the same aggregate particles, however, on their opposite sides than in the experiment. The crack propagated near the large aggregate in the specimen's mid-height on the right side instead of breaking it on the left side. The bottom part of the crack was narrow and straight as in the experiment, however, the crack propagated on the left side of the large aggregate, opposite to the experiment wherein it followed the right edge of the aggregate (Fig.9Ac). In addition, the crack was more curved. The large aggregate at the mid-height of the specimen was also broken in the experiment. The top of the specimen was crushed in the experiment that was reproduced in DEM as intensive micro-cracking of the cement matrix under the loading board (Fig.9Aa) and wider crack opening. In the small specimen, some fine differences in the aggregate shape and pores' position greatly influenced the crack pattern. Moreover, the 3D aggregate arrangement influenced the crack shape. To obtain a more realistic crack pattern, the 3D DEM simulations should be carried out [16]. The cracks computed in DEM for D=150 mm were more realistic as compared to the experiment (Fig.9B). For D=150 mm, no aggregate breakage occurred in the experiment (Fig.9Ba) Note that the crushed piece of the specimen separated during transportation (Fig.9Ba). The same crack's shape was reproduced in DEM as to the crack's branching at the specimen top (Fig.9Bb-c). The main crack followed the left side of large aggregate in the specimen's mid-height, however, another branching appeared at the specimen bottom (Fig.9Bc) with a finer crack that propagated at the same side of the aggregate as in the experiment. Finally, the largest specimen D=250 mm was almost symmetrically cracked in DEM while in the experiment, it was curved to the right side (Fig.9Cc) probably due to a small load eccentricity. The crack was curved to the left at the specimen top, both in the experiments and DEM, forming a wedge connecting the straight part of the crack with the loading strip edge (Fig.9Ca-c). The similar behaviour was obtained in the specimen's mid-height wherein the crack in DEM was curved to the left (Fig.9Cb-c). Even though, the macro-crack developed along other aggregate particles, it had a very small width in the specimen mid-height and was branched with various micro-cracks at the specimen bottom and top as in both the experiment and DEM (Fig.9Ca-c). The intense cracking at the top and bottom (the wedges) and multiple micro-cracking in the cement matrix were obtained in the model.

The macroscopic DEM results of the strength (Fig.10) and angle α between the inclination of softening and horizontal axis and (Fig.11) from the experiments were directly compared with the DEM results. The strength reduction was very similar in the experiment and DEM for the specimens D=150 mm and D=250 mm. The size effect on brittleness (defined as the angle α between the softening inclination to the horizontal) was stronger in DEM than in the experiment. For the smallest specimen, the softening angle in DEM was equal to the mean angle in experiment (α=78°) whereas for the specimens D=150 mm and D=250 mm was equal to α=95° and α=106° in the experiments and α=102° and α=120° in the numerical calculations (the difference 7%-13%).

4 CONCLUSIONS

The experimental size effect was realistically reproduced in DEM calculations at the aggregate level, i.e. the concrete strength and ductility decreased with increasing concrete specimen diameter. The calculated decreasing strength approached an asymptote with increasing cylindrical specimen diameter within the considered specimen size range.

DEM proved its capability to model concrete fracture in detail by taking the snap-back instability into account. The agreement of calculated stress-displacement results and crack shapes with experimental ones was satisfactory.

The crack volume and average crack width decreased with increasing specimen diameter due to crack branching.

Acknowledgements

The research work has been carried out within the project: ''*Innovative ways and effective methods of safety improvement and durability of buildings and transport infrastructure in the sustainable development*'' financed partly by the European Union POIG.01.01.02-10-106/09-01) and the project ‘‘*Experimental and numerical analysis of coupled deterministic-statistical size effect in brittle materials*” financed by the National Science Centre NCN (UMO-2013/09/B/ST8/03598).

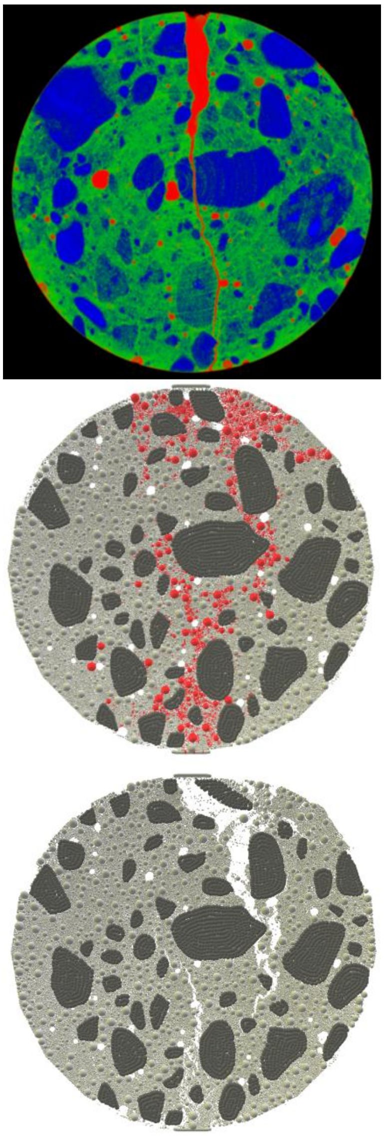

A)

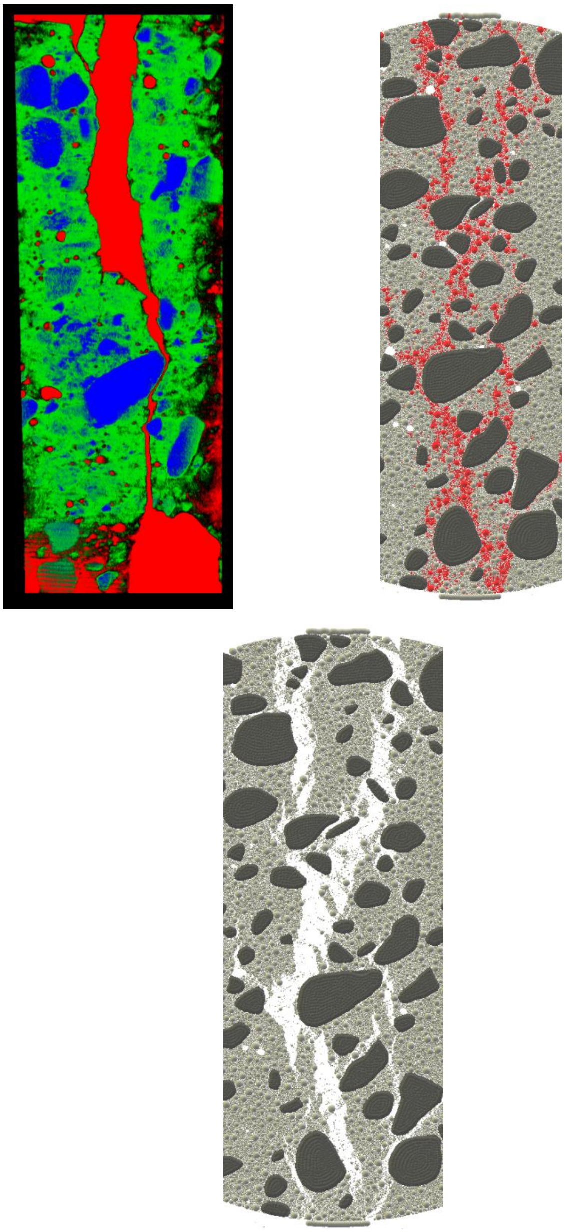

B)

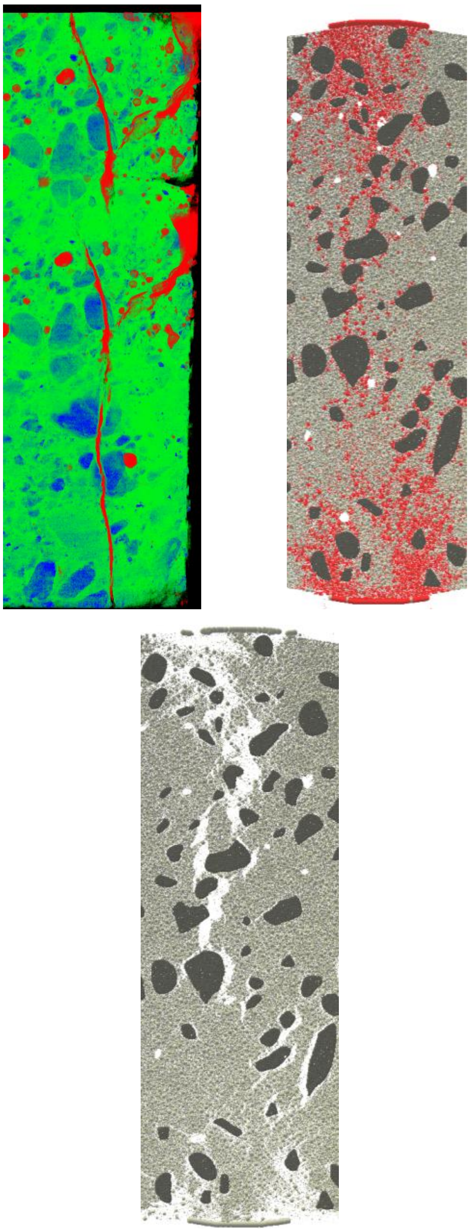

C)

Figure 9: Crack geometry (micro-CT images, broken contacts in red in DEM, deformed specimens in DEM) for different specimen diameters *D:*
A) *D*=74 mm, B) *D*=150 mm and C) *D*=250 mm.

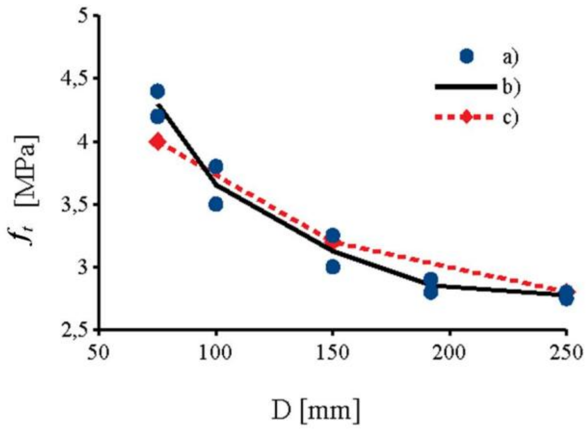

Fig.10: Comparison of experimental and numerical results of tensile splitting strength *ft* against specimen diameter *D* for: a) each specimen (dots), b) mean value trend (continuous line) and c) DEM result (dashed line).

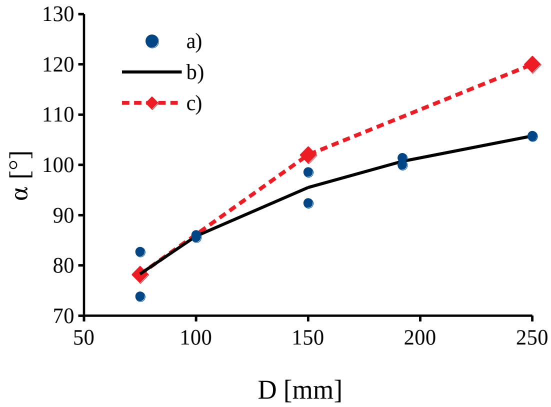

Figure 11: Softening parameter *α* versus specimen diameter *D* for each concrete specimen in tensile splitting test.

REFERENCES

[1] Suchorzewski, J., Tejchman, J. and Nitka, M. 2018. Experimental and numerical investigations of concrete behaviour at meso-level during quasi-static splitting tension. *Theoretical and Applied Fracture Mechanics* 96: 720-739.

[2] Bažant, Z.P., Kazemi, M.T., Hasegawa, T., Mazars, J. 1991. Size Effect in Brazilian Split-Cylinder Tests: Measurements and Fracture Analysis, *ACI Material Journal* 325 -332.

[3] Hasegawa, T., Shioya, T. and Okada, T. 1985. Size effect on splitting tensile strength of concrete, Proceedings, Japan Institute 7th

Conference, 309-312.

[4] Carmona, S., Gettu, R. and Aguado, A. 1998. Study of the post-peak behaviour of concrete in the splitting-tension test, Fracture Mechanics of Concrete Structures, Proceedings FRAMCOS-3, Aedificatio Publishers, D-79104 Freiburg, Germany 111-120.

[5] Kadlecek, V. Sr., Modry, S., Kadlecek, V. Jr. 2002. Size effect of test specimens on tensile splitting strength of concrete: general relation, *Materials and Structures* 35, 28-34.

[6] Torrent, R.J. 1977 A general relation between tensile strength and specimen geometry for concrete - like materials. *Materials and Structures* 10: 187-196.

[7] Skarzyński, Ł., Tejchman, J. 2016. Experimental investigations of fracture process in concrete by means of x-ray micro-computed tomography. *Strain* 52: 26-45.

[8] Skarżyński, Ł., Marzec, I., Tejchman, J. 2019. Fracture evolution in concrete compressive fatigue experiments based on X-ray micro-CT images. *International Journal of Fatigue* 122 (2019), 256–272.

[9] Skarzynski, Ł., Nitka, M. and Tejchman, J. 2015. Modelling of concrete fracture at aggregate level using FEM and DEM based on x-ray micro-CT images of internal structure. *Engineering Fracture Mechanics* 147:13-35.

[10] Vorechovsky, M. 2007. Interplay of size effects in concrete specimens under tension studied via computational stochastic fracture mechanics. *International Journal of Solids and Structures* 44: 2715–2731.

[11] EN12390-6:2012 – European standard Testing hardened concrete Part 6: Tensile splitting strength of test specimens, European Committee for Standardization, 2012.

[12] Rocco, C., Guinea, G.V., Planas, J., Elices, M. 1999. Size effect and boundary conditions in the Brazilian test: Experimental verification. *Materials and Structures* 32: 210-217.

[13] Bažant, Z.P., Planas, J. *Fracture and size effect in concrete and other quasi-brittle materials.* CRC Press LLC (1998).

[14] Xiao, J., Wengui, L., Zhihui, S. et al. 2013. Properties of interfacial transition zones in recycled aggregate concrete tested by nanoindentation. *Cement & Concrete Composites* 37: 276-292.

[15] Nitka, M., Tejchman, J. 2015. Modelling of concrete behaviour in uniaxial compression and tension with DEM. *Granular Matter* 17(1): 145-164.

[16] Nitka, M., Tejchman, J. 2018. A three-dimensional meso scale approach to concrete fracture based on combined DEM with X-ray μCT images. *Cement and Concrete Research* 107, 11-29